

Resonant coherent excitation of channeled ions

C. D. Moak, S. Datz, O. H. Crawford, H. F. Krause, P. F. Dittner, J. Gomez del Campo, J. A. Biggerstaff, P. D. Miller, P. Hvelplund,* and H. Knudsen*

Oak Ridge National Laboratory, Oak Ridge, Tennessee 37830

(Received 6 September 1978)

The hydrogenlike ions B^{4+} , C^{5+} , N^{6+} , O^{7+} , and F^{8+} , and the heliumlike ion F^{7+} have been shown to exhibit resonant coherent excitation from the atomic level $n = 1$ to $n = 2$, caused by the periodic potential oscillations which occur as the ion moves in axial and nearly axial planar channels in thin crystals of Au and Ag. Various harmonics of the lattice-string periodicity are effective, at certain critical ion velocities, in reducing the number of one-electron ions which survive passage through the crystal without electron loss. Resonances, appearing as minima in the one-electron charge-state fraction versus velocity, have been found for several axial channels and for several different harmonics of the string frequencies. In some cases the resonances can be split by small crystal tilts which produce sidebands upon the string frequency. Certain harmonics have been shown to produce tilt-insensitive double minima which measure Stark splittings of the $n = 2$ levels.

I. INTRODUCTION

Coherent interactions between moving charged particles and a spatially periodic potential at rest in the laboratory have been observed in a variety of experiments. Electron-diffraction phenomena are illustrative of these interactions. In an early experiment it was demonstrated that relativistic electrons can cause the emission of visible light from localized surface charges induced to move across a metallic grating by grazing electrons. The wavelength versus angle of observation and versus electron velocity were demonstrated to be correctly predicted; the phenomenon is known as the Smith-Purcell effect.¹ In this case the light is considered to be emitted by the grating. Smith and Purcell reported observation of light corresponding to harmonics of the fundamental frequency of the grating spacing, up to order five. Dyson and Überall pointed out that very high-energy electrons moving in crystal lattices would exhibit coherence effects that would alter the energy spectra of bremsstrahlung and electron-positron pairs.² Überall reported on quantitative estimates of the enhancements to be expected in the energy distributions for pairs and bremsstrahlung due to lattice periodicity.³ In 1965, Okorokov proposed the possibility of coherent excitation of optical spectra⁴ and coherent nuclear Coulomb excitation⁵ for atoms passing along crystalline channels. Okorokov's analysis contained the prediction that the crystal atomic strings would provide excitation at the atomic string frequency, v/d , and the overtones of that frequency. In addition it was predicted that thermal motion of the atoms of the crystal would remove harmonics of order greater than ten for crystals at room temperature.

The first experimental use of macroscopic spatially periodic electric fields to produce velocity-dependent frequency tuning to cause atomic transitions in a moving ion was reported by Hadeishi *et al.*^{6,7} In this case comb-shaped electrodes were used to set up spatially periodic fields which produced resonant transitions between the ($3^2S_{1/2} - 3^2P_{1/2}$) levels in hydrogen atoms as the velocity of the atoms was tuned. The first report of the use of spatially periodic fields in a crystal lattice to cause atomic transitions in a moving ion was given by Okorokov *et al.*⁸ The atomic transition was from $n=1$ to $n=4$ in singly ionized helium. The ions were accelerated and passed through a $\langle 100 \rangle$ axial channel of a silver crystal 1100 Å thick. The $n=4$ to $n=3$ transition in the emerging ions ($\lambda = 4685$ Å) was used to detect the presence of $n=4$ He⁺ in the emerging beam. Near the calculated resonance velocity for tuning the $n=1$ to $n=4$ transition, a peak in 4685-Å light output of the beam was reported and it was reported that a 5° misalignment of the crystal caused the peak to disappear. Since that time, a number of attempts have been made to observe resonant coherent excitation of He⁺ without success. One report of positive findings by Gaillard *et al.*⁹ was followed by an investigation with improved apparatus by Poizat and Gaillard.¹⁰ The earlier findings could not be reproduced. Initially they had reported a very strong maximum near resonance velocity for He⁺ ions passing along $\langle 110 \rangle$ axial channels of a thin gold crystal; again the $n=4$ to $n=3$, 4685-Å light was plotted versus velocity.

A quantum-mechanical calculation of excitation probability for an ion moving in a crystal was reported by Kondo.¹¹ Theoretical estimates were given by Kalashnikov and Pankratov for the com-

petition between excitation by harmonics of a lattice frequency and excitation by a multi-“photon” process¹²; they reported that the multi-“photon” process should be 100 times weaker than excitation by harmonics for the case of second-harmonic excitation of He^+ . Shindo and Ohtsuki have predicted that coherent excitation resonances might be so broad that different harmonic peaks might overlap, making detection of such resonances difficult.¹³ Berry *et al.*¹⁴ performed several different experiments designed to broaden the scope of the search. First they looked for resonances for He^+ ions along the $\langle 111 \rangle$ axis in 400-Å-thick Au crystals. No effect greater than ~2% was observed in the yield of the 4685-Å light. In addition no resonance was observed for the various charge state fractions of the emerging He ions. Berry *et al.* pointed out that the “diameter” (~8 Å) of the $n=4$ state of He^+ is considerably larger than the size of the $\langle 100 \rangle$, $\langle 100 \rangle$, or $\langle 111 \rangle$ channels of Ag or Au. Such a state would be expected to be at a different energy from the level position in free space, and the probability of ionization should be very large, leading to removal of the electron rather than subsequent light emission. A resonance in the He^{++} fraction might be expected to be a more sensitive indicator of resonant coherent excitation, but no resonance was found. An attempt was made to find a resonance with a “smaller” ion. The state chosen was the $2s3p^3P(50.3 \text{ eV})$ level in N^{3+} , which decays with a photon at $\lambda=3480 \text{ Å}$. A 530-Å-thick Au crystal was used and no resonances were found for the $\langle 110 \rangle$, the $\langle 100 \rangle$, or the $\langle 111 \rangle$ axis. Berry *et al.* then attempted to find resonances with He^+ in the $\langle 110 \rangle$ channels (and later with other channels¹⁵) of Au and none were found. Most recently Mannami *et al.*¹⁶ have reported that they find no evidence for resonances for He^+ ions in the $\langle 111 \rangle$ axis of Au and they have estimated their limits of detectability at one part in a thousand. We are aware of work performed at Bell Telephone Laboratories, wherein a careful search showed no resonances for the $n=1 \rightarrow n=4$, $n=4 \rightarrow n=3$ photon yield from He^+ .¹⁷ An attempt has been made by Burch and Marwick to find a resonance for the $n=1 \rightarrow n=2$ transition in C^{5+} channeled in the $\langle 110 \rangle$ axis in gold but no resonances were found.¹⁸ In a previously published letter we showed that resonant excitation does indeed occur and can be observed if the ion is maintained in a well-defined charge state in the crystal and if the observations are limited to the best channeled particles.¹⁹

II. DESCRIPTION OF EFFECTS

Ideal conditions for observation of resonant coherent excitation would occur for a one-electron

ion which could, off resonance, remain fixed in charge state and remain in its atomic ground state while passing through the crystal. Assuming that, at resonance, the disturbance due to the crystal gives coherent excitation of an atomic state transition, it would be desirable if (i) all the excited ions would be ionized in the crystal and subsequent charge-state analysis could be used to detect charge state transitions at resonance, or (ii) all the excited ions would remain in that state of excitation until they could decay by photon emission and photon detectors would be used to detect the resonant excitation.

In the experiments reported here we have used the charge-state transition method. A monoenergetic beam of perfectly collimated one electron ions, perfectly aligned to an ideal crystal will uniformly illuminate ~ 10^{13} sets of atomic strings in each mm^2 of specimen area and some of these particles will enter near a string of atoms and will be dechanneled. Others will remain channeled but will come close enough to change their charge rapidly in close encounters with the crystal atoms. Some of the ions may retain their charge integrity. Earlier studies have shown that for zero-, one-, and two-electron oxygen ions at 27.8 and 40 MeV, part of the channeled ions retain their charge state through as much as 10^4 Å in Ag crystals.²⁰ The same effect has been observed for planar channeling of ions with $5 \leq Z \leq 9$ in Au.²¹ The ions which retain a fixed charge state through the crystal exhibit a characteristic energy loss which can be distinguished in the energy-loss spectrum as shown in Fig. 1. In the figure, zero-, one-, and two-electron ions of oxygen show significant differences in energy loss. Each spectrum contains a group whose energy loss varies as q^2 , where q is ion charge. Some of these fixed-charge-state ions may become excited by valence-electron bombardment, but there will be a group which traverses the crystal in the ground state. We will show that this group can be coherently excited by a crystal lattice and, following excitation, these ions more readily lose an electron. The objective of the experiments reported here was to measure the surviving fraction of one-electron ions which had been well channeled (as indicated by their characteristic energy loss) along a crystal axis, and to search for minima at expected resonance velocities.

A channeled ion passing between ordered rows of atoms in a crystal lattice with a velocity v experiences a coherent periodic perturbation of fundamental frequency $\nu = v/d$, where d is the distance between atoms in a string. In general, the perturbation is not a pure sine wave; the perturbation consists of periodic sharp maxima in the

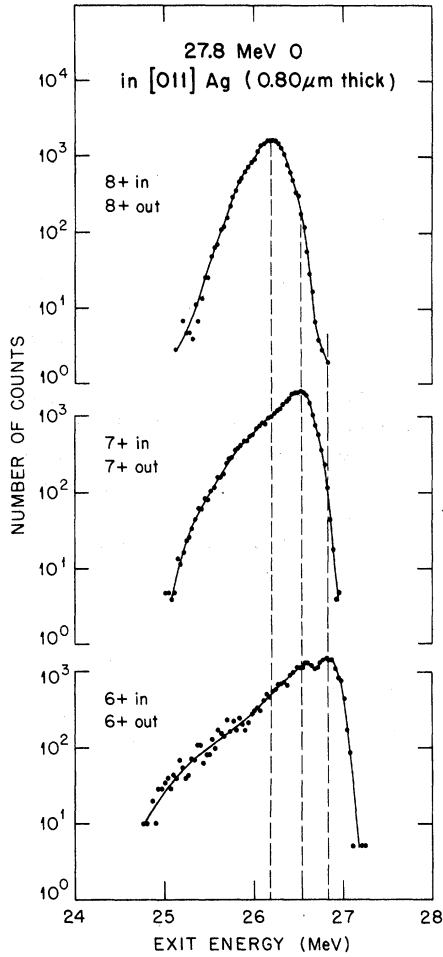


FIG. 1. Energy spectra of 27.8 MeV oxygen ions emerging from the [011] channel of Ag.

electric field, and thus it contains many harmonics of the fundamental string frequency so that the general expression becomes

$$\nu = K(v/d); K = 1, 2, 3, \dots \quad (1)$$

When one of these frequencies coincides with

$$\nu_r = \Delta E_{ij}/h, \quad (2)$$

where ΔE_{ij} is the energy difference between two electronic states i and j of the ion, a resonant coherent excitation might occur. For the particular case of the one electron ion, the energy difference, neglecting relativistic effects, and crystal field effects, is

$$\Delta E_{ij} = (i^{-2} - j^{-2})Z_1^2 e^2 / 2a_0. \quad (3)$$

For the case $i=1$ and $j=2$ two convenient numerical expressions are

$$E_r \text{ (MeV/amu)} = 3.03 K^{-2} d_A^2 (\Delta E_{\text{kev}})^2 \quad (4)$$

and

$$E_r \text{ (MeV/amu)} = 3.15 \times 10^{-4} K^{-2} d_A^2 Z_1^4. \quad (5)$$

For example, for C^{5+} in the $\langle 100 \rangle$ axial channel of Au ($d_A = 4.07897$ at 25°C)²² and for $K=1$, Eq. (5) gives 6.8 MeV/amu, or an ion energy of 81.6 MeV. The second harmonic occurs at 20.4 MeV. For heavy ions, where relativistic effects cannot be neglected, exact values should be used for ΔE_{kev} in Eq. (4).

For relativistic velocities, Eq. (1) should be replaced by

$$\nu = K(v/d)\gamma; K = 1, 2, 3, \dots, \quad (1')$$

where ν is the frequency in the frame of the moving ion and

$$\gamma = (1 - v^2/c^2)^{-1/2}.$$

Taking into account that the translational energy is $\mu c^2(\gamma - 1)$, where μ is the rest mass, we find, in place of Eq. (4),

$$E_r \text{ (MeV/amu)} = 3.03 K^{-2} d_A^2 (\Delta E_{\text{kev}})^2 [2/(1 + \gamma)]. \quad (4')$$

III. THEORY

In this section, we attempt to describe coherent transitions between the low-lying electronic states of channeled one-electron ions in the simplest physically realistic approximation. These ions are assumed to follow classical trajectories along which they experience oscillating electric fields, which, under certain conditions, induce coherent transitions. The energy levels are not quite the same as in the vacuum, being perturbed by the electric potential of the crystal. Therein lies part of the interest: the observed energy shifts and splittings provide a measure of the interaction. The electrostatic potential increases with displacement from the center of a channel, so the potential energy of an electron decreases. This potential lowers the electronic levels of the channeled ions. Since the higher-energy orbitals extend further, they are affected more than the ground state and the result is a decrease in the energy difference between levels. Therefore, one expects the transition energies to be smaller than the vacuum values. Stark splittings are caused by the field due to polarization of the medium (the wake field).²³

After a specification of the model, we devote the remainder of this section to the frequency and polarization of the fields sensed by ions moving along various crystallographic directions. Theoretical calculations of the perturbed energy levels,²⁴ and a more complete dynamical treatment including ionization,²⁵ will be published separately.

Consider the space spanned by the 1s, 2s, and

the three $2p$ hydrogenic states, and assume a Hermitian effective Hamiltonian of the form

$$H = H^{(0)} + V_{\text{avg}}^{(1)} + V_{\text{osc}}^{(1)}, \quad (6)$$

in which $H^{(0)}$ is the unperturbed (hydrogenic ion) Hamiltonian, and the $V^{(1)}$ terms contain the interaction with the crystal's electric potential, $V^{(1)}$ being the time average (along a trajectory) of the interaction, and $V^{(1)}$ being its oscillation with time.

It is convenient to write the wave function in the form

$$\psi = \sum_{\nu=1}^5 |\nu\rangle C_{\nu}(t) \exp(-iE_{\nu}t/\hbar), \quad (7)$$

in which $|\nu\rangle$ and E_{ν} are the orthonormal eigenfunctions and eigenvalues of the time-independent part of the Hamiltonian in the space spanned by the above basis:

$$\langle \mu | H^{(0)} + V_{\text{avg}}^{(1)} | \nu \rangle = E_{\nu} \delta_{\mu\nu}. \quad (8)$$

Then, the time-dependent Schrödinger equation reduces²⁶ to the following coupled differential equations for the amplitudes $C_{\mu}(t)$

$$\frac{dC_{\mu}}{dt} = \frac{1}{i\hbar} \sum_{\nu=1}^5 \langle \mu | V_{\text{osc}}^{(1)} | \nu \rangle C_{\nu} \exp\left(\frac{i(E_{\mu} - E_{\nu})t}{\hbar}\right), \quad (9)$$

where $\mu = 1, 2, \dots, 5$.

The physical picture suggested by this treatment is that the time-independent interaction $V_{\text{avg}}^{(1)}$ modifies the stationary states of the ion, so that they become $|\mu\rangle$ with energies E_{μ} , $\mu = 1-5$. The oscillating part $V_{\text{osc}}^{(1)}$ of the interaction induces transitions between these modified states.

We are concerned with the situation in which the transition probability upon traversing one unit cell is quite small, so that the probability only becomes significant when constructive interference occurs along a segment of trajectory through several unit cells. Such constructive interference requires that $\langle \mu | V_{\text{osc}}^{(1)}(t) | \nu \rangle$ contain a Fourier component at an angular frequency close to $\Delta E/\hbar$, where ΔE is the transition energy [so that the phase of the $\nu \rightarrow \mu$ term in the right-hand side of Eq. (9) is slowly varying].

To proceed to specific cases, it is convenient to approximate $V_{\text{osc}}^{(1)}$ as the interaction of the electron with a field $\vec{E}(t)$ which (while varying with time due to the motion of the ion) is constant over the range of the atomic orbital²⁷:

$$V_{\text{osc}}^{(1)} \approx -e\vec{r} \cdot \vec{E}(t) \\ = -exE_x(t) - eyE_y(t) - ezE_z(t), \quad (10)$$

where \vec{r} (with Cartesian coordinates x, y, z) is the

position of the electron relative to the nucleus. Then, Eq. (9) becomes

$$\frac{dC_{\mu}}{dt} = -\frac{e}{i\hbar} \sum_{\nu=1}^5 [\langle \mu | x | \nu \rangle E_x(t) + \langle \mu | y | \nu \rangle E_y(t) + \langle \mu | z | \nu \rangle E_z(t)] C_{\nu} \exp\left(\frac{i(E_{\mu} - E_{\nu})t}{\hbar}\right), \quad (11)$$

and we have only electric dipole²⁷ transitions.

It follows that if, for example, the symmetry and the coordinates are such that one of the excited states is simply $2p_x$, then the coherent $1s - 2p_x$ transition proceeds only if there is a component of the field having both (i) frequency $\omega \approx (E_{2p_x} - E_{1s})/\hbar$ and (ii) a nonzero projection in the x direction.

A. Spectral analysis of the field

We require spectral analyses, for the various channels of interest, of the electric field at the centers of moving ions. If a crystal's electrons (and nuclei) responded adiabatically (or not at all) to the ion, this field would be, by the Hellmann-Feynman theorem,²⁸ equal to the negative gradient, with respect to the ion's position (U, V, W), of the potential $\phi(U, V, W)$ at the center of the ion. Furthermore, ϕ would be independent of the velocity of the ion. In the present case, the adiabatic approximation is invalid for some of the electrons, the consequence being a velocity-dependent polarization wake.²³ However, the variation with time of the wake field, in the ion's moving frame of reference, is presumably small (as discussed in a later paper),²⁴ and may be ignored for the present purpose. We therefore consider the field which causes the coherent transitions to be minus the gradient of the potential function $\phi(U, V, W)$.

For a simple face-centered cubic crystal, place the origin on an atom, and define orthogonal U, V , and W axes directed toward corners of a cubic unit cell. In this communication we use the following conventions in describing axial and planar channels: Specific particular axes are written as, e.g., $[001]$, $[010]$, etc. Specific planar channels are written as, e.g., (100) , (010) , etc. When the order of the indices is unimportant, axes are written as, e.g., $\langle 001 \rangle$ or $\langle 100 \rangle$, and for planar channels, e.g., $\{100\}$. Since the potential ϕ depends only on position, it must be periodic with period a (the lattice constant) in each of U, V , and W , and therefore may be written as a triple Fourier sum. Because of the reflection symmetry at the origin, there are no sine terms, and we have

$$\phi(U, V, W) = \sum_{hki} \phi_{hki} \cos\left(\frac{2\pi hU}{a}\right) \cos\left(\frac{2\pi kV}{a}\right) \cos\left(\frac{2\pi lW}{a}\right). \quad (12)$$

The indices run over all non-negative integers, but, because of the symmetry of the face-centered cubic lattice, the only nonzero coefficients ϕ_{hki} are those in which the indices are either all even or all odd.²⁹

We are now ready to analyze the oscillating field sensed by ions moving along specific trajectories. In each case, the discussion will emphasize the paths nearest the center of the channel because (i) our beam and detector collimation permits only those ions deflected by $\approx 3 \times 10^{-4}$ radians to be detected (see apparatus, Sec. IV), discriminating against ions which closely approach a string in the crystal, and (ii) these trajectories best explain the origin of the dominant features of the velocity dependence of the coherent excitation. These features are expected to arise from the ions which experience the longest coherence times (reasoning from $\Delta E \geq \hbar/\Delta t$), by staying farthest from the atoms of the crystal. The relative contribution of the best channeled ions (especially the hyperchanneled ions)³⁰ will be discussed in a later section.

B. The [001] axial channel

The [001] axial channels are centered along the line $(U, V) = (\frac{1}{4}a, \frac{1}{4}a)$ and equivalent lines. For simplicity, assume the following straight-line trajectory parallel to the channel axis:

$$E_w(l) = \frac{2\pi l}{a} \sum_{hki} (-1)^{\frac{1}{2}(h+k)} \phi_{hki} \begin{cases} \cos(2\pi hb_U/a) \cos(2\pi kb_V/a), & l \text{ even} \\ (-1) \sin(2\pi hb_U/a) \sin(2\pi kb_V/a), & l \text{ odd} \end{cases}, \quad (18)$$

where the upper factor in each case is used for even indices, and the lower factor for odd ones. (Recall that the only nonzero ϕ_{hki} are those in which h , k , and l are *all* even or *all* odd.) In this case, where the beam is parallel to the [001] axis, $K = l$.

Equation (15) describes a set of frequencies consisting of harmonics of a single fundamental frequency, with the index l distinguishing the harmonics, and a constant component. Since the atom-to-atom distance along the "strings" is a in this case, the result agrees with Eq. (1).

The impact parameter dependence of the electric field, as displayed in Eqs. (16)–(18), differs according to both the direction of the field, and

$$\begin{aligned} U &= \frac{1}{4}a + b_U, \\ V &= \frac{1}{4}a + b_V, \\ W &= vt, \end{aligned} \quad (13)$$

where b_U and b_V are (constant) impact parameters relative to the center of the channel, and v is the velocity. To obtain the electric field, we take the gradient of the right-hand side of Eq. (12), change the sign, and substitute Eq. (13) for the coordinates. We find

$$\begin{aligned} E_U &= \sum_l E_U(l) \cos(\omega_l t), \\ E_V &= \sum_l E_V(l) \cos(\omega_l t), \\ E_W &= \sum_l E_W(l) \sin(\omega_l t), \end{aligned} \quad (14)$$

in which

$$\omega_l = (2\pi lv/a), \quad l = 0, 1, 2, 3, \dots, \quad (15)$$

$$E_U(l) = \sum_{hki} (-1)^{\frac{1}{2}(h+k)} \frac{2\pi h}{a} \phi_{hki} \times \begin{cases} \sin(2\pi hb_U/a) \cos(2\pi kb_V/a), & l \text{ even} \\ \cos(2\pi hb_U/a) \sin(2\pi kb_V/a), & l \text{ odd} \end{cases}, \quad (16)$$

$$E_V(l) = \sum_{hki} (-1)^{\frac{1}{2}(h+k)} \frac{2\pi k}{a} \phi_{hki} \times \begin{cases} \cos(2\pi hb_U/a) \sin(2\pi kb_V/a), & l \text{ even} \\ \sin(2\pi hb_U/a) \cos(2\pi kb_V/a), & l \text{ odd} \end{cases}, \quad (17)$$

and

whether the harmonic index l is even or odd. In particular, for trajectories sufficiently close to the center of the [001] channel, Eqs. (16)–(18) imply that, for even l , $E_W(l)$ is much larger in absolute value than $E_U(l)$ and $E_V(l)$, while for odd l , the largest component is $E_U(l)$ or $E_V(l)$; in other words, for approximately centered trajectories, the even harmonics of the field are predominantly longitudinal, while the odd harmonics are mainly transverse. Moreover, along a path precisely down the center of the [001] channel, the odd harmonics vanish altogether.

In general, E_U and E_V are in phase, so the transverse component of the field has only one direction, which is approximately away from the

closest string of atoms. However, the longitudinal component E_w is 90° out of phase with the others in time. The field is therefore elliptically polarized.

To get further information about the oscillating field, including its impact parameter dependence, we have computed the coefficients $E_V(l)$, $E_V(l)$, and $E_w(l)$ for several trajectories parallel to the [001] axis. Similar calculations have been made for other axial channels. We approximate the potential as a sum of atomic potentials ϕ_a , using Molière's approximation³¹ to the Thomas-Fermi potential

$$\phi_a(\mathbf{r}) = \frac{eZ_2}{r} \sum_{j=1}^3 \alpha_j \exp(-\beta_j r/a_{TF}), \quad (19)$$

where $\{\alpha\} = \{0.1, 0.55, 0.35\}$, $\{\beta\} = \{6.0, 1.2, 0.3\}$, $Z_2 = 79$ (atomic number of gold), and $a_{TF} = 0.8853 Z_2^{-1/3}$ Bohr radii (the Thomas-Fermi screening length). The potential $f^{(i)}$ due to the i th string has a Fourier expansion of the form

$$f^{(i)}(\rho_i, z_i) = \sum_m f_m(\rho_i) \cos(2\pi m z_i/d), \quad (20)$$

where ρ_i is the distance from the string, z_i is the distance along it, measured from one of the atoms, and d is the atom-to-atom distance. The coefficients in the above equation are given by³²

$$\begin{aligned} f_m(\rho_i) &= \frac{2}{1 + \delta_{m0}} \int_{-\infty}^{\infty} \phi_a(z^2 + \rho_i^2)^{1/2} \cos(2\pi m z/d) dz \\ &= 4Z_2 e [(1 + \delta_{m0})d]^{-1} \\ &\quad \times \sum_{j=1}^3 \alpha_j K_0 \left\{ \rho_i \left[\left(\frac{\beta_j}{a_{TF}} \right)^2 + \left(\frac{2\pi m}{d} \right)^2 \right]^{1/2} \right\}, \end{aligned} \quad (21)$$

in which $K_0\{\}$ is a modified Bessel function of order zero. To calculate the field, for a given trajectory (i.e., given impact parameters), we compute the longitudinal and transverse components of the negative gradient of Eq. (20), for each string, and sum vectorially over the strings. Phase shifts are required, since atoms in the strings are, in most channels, displaced longitudinally with respect to the atoms of neighboring strings.

The results of the Molière potential calculation for <001> axial channeling are shown in Fig. 2. The trajectories are symmetrically chosen ones which, on the left-hand side of the figure, are closer to one string than to any other, and, on the right-hand side, are equally close to two strings, as depicted in the inset. This figure shows significant differences between the even and odd harmonics of the field. It was argued above that the

even and odd harmonics are predominantly longitudinal and transverse, respectively, for (hyperchanneling) trajectories well-centered in the <001> channel. We see now that the same polarizations persist all the way across the right-hand side of Fig. 2, even where the ion is passing into the adjacent channel. This strongly suggests that the even-odd dichotomy predicted for <001> hyperchanneling should occur for ordinary axial channeling, as well. Those trajectories which approach a single string in a symmetric way are exceptions to the rule, according to the curves in the left-hand side of Fig. 2.

As would be expected, superimposed upon the even-odd differences is a rapid decrease in the field components with increasing harmonic index, a trend which is strongest near the center of the channel. (Note the different scales on each ordinate.)

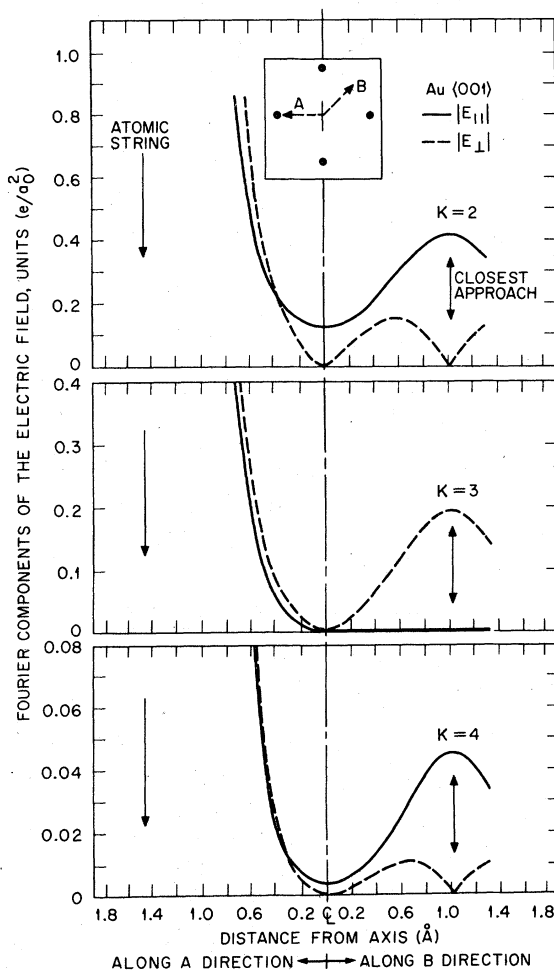


FIG. 2. Fourier coefficients of the longitudinal and transverse components of the electric field calculated for trajectories parallel to <001> axis versus displacement from channel center line.

C. The $\langle 111 \rangle$ axial channels

The $\langle 111 \rangle$ axial channel is bounded by an equilateral array of three strings of atoms. In each string, the distance d between atoms is $\sqrt{3}a$, so the frequencies ω_K are $2\pi K v / (\sqrt{3}a)$, $K=1, 2, 3, \dots$

Atoms in each string are displaced along the channel direction by $\pm \frac{1}{3}d$ with respect to those in the nearest-neighboring strings. Therefore, for trajectories exactly along the center of the channel, the field harmonics which are divisible by three are longitudinal, while the others are transverse (and are circularly polarized). In the latter case, the field rotates clockwise in half the $\langle 111 \rangle$ channels, and counterclockwise in the other half.

Electric field components computed from the Molière potential for gold in the manner described in connection with $\langle 001 \rangle$ channels, are shown in Fig. 3. The difference between the fourth and fifth

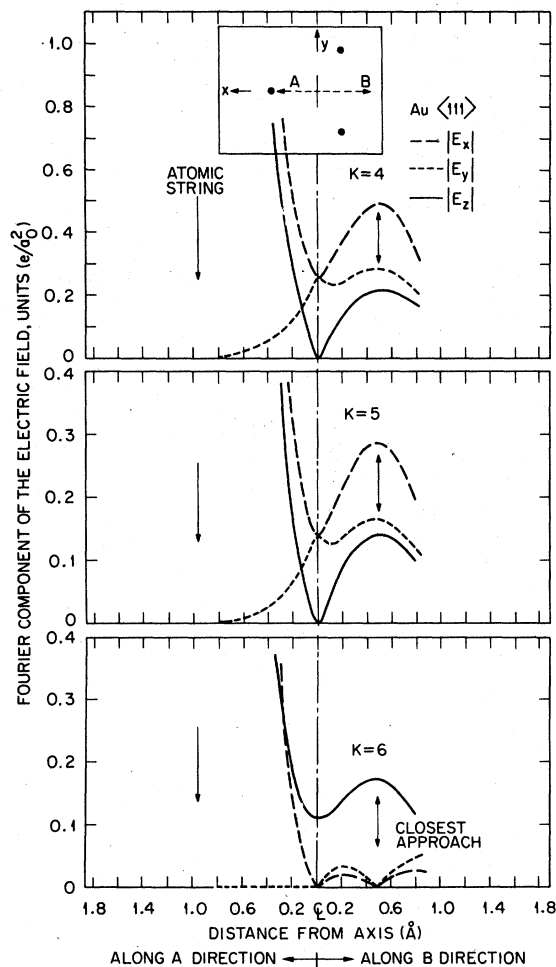


FIG. 3. Fourier coefficients of the longitudinal and transverse components of the electric field calculated for trajectories parallel to $\langle 111 \rangle$ axis versus displacement from channel center line.

harmonics on the one hand, and the sixth on the other, is a good illustration of the divisible-by-three rule for $\langle 111 \rangle$ channels. The right-hand side of the figure shows, furthermore, that the prediction made above for the field polarization at the center of the channel holds for ordinary $\langle 111 \rangle$ axial channeling as well, assuming the passage is made in a quite symmetric fashion. However, the left-hand side of the figure warns of possible exceptions, as the $K=6$ polarization changes from longitudinal to transverse when the ion moves only $\sim 0.3 \text{ \AA}$ from the channel center toward one string.

D. The $\langle 110 \rangle$ axial channels

The $\langle 110 \rangle$ axial channel is bounded by four strings arranged at the corners of a rhombus, as shown in the inset of Fig. 4. The atom-to-atom distance d in each string is $a/\sqrt{2}$, so the angular frequencies are $2\sqrt{2}\pi K v / a$, $K=1, 2, 3, \dots$

Atoms in the adjacent strings are displaced in the channel direction by $\pm \frac{1}{2}d$. In this respect, the channel resembles the $\langle 001 \rangle$ which is more symmetric. For paths down the center of a $\langle 110 \rangle$ channel, the oscillating field is longitudinal for all harmonics. This is illustrated in Fig. 4, which shows the second and third harmonics, calculated

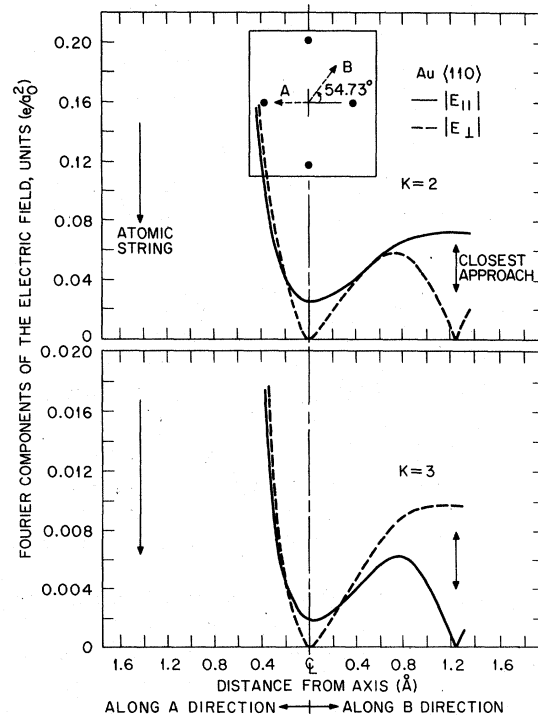


FIG. 4. Fourier coefficients of the longitudinal and transverse components of the electric field calculated for trajectories parallel to $\langle 110 \rangle$ axis versus displacement from channel center line.

from the Molière potential, Eq. (19), by the method described earlier.

E. (100) planar channeling near the [001] direction

Consider channeling in the (100) plane, on a straight line making an angle θ with the W (or [001]) axis. The center of the channel is the $U = \frac{1}{4}a$ plane (and other equivalent ones), and we suppose the ion to travel a fixed distance b_U from said midplane. The trajectory is therefore

$$W = vt \cos \theta, \tag{22}$$

$$V = vt \sin \theta, \tag{23}$$

$$U = \frac{1}{4}a + b_U. \tag{24}$$

It follows from Eqs. (16)–(18) that the three components of the field are

$$E_U = \sum_{lk} E_U(l, k) (\cos \omega_{lk}^+ t + \cos \omega_{lk}^- t), \tag{25}$$

$$E_W = \sum_{lk} E_W(l, k) (\sin \omega_{lk}^+ t + \sin \omega_{lk}^- t), \tag{26}$$

and

$$E_V = \sum_{lk} E_V(l, k) (\sin \omega_{lk}^+ t - \sin \omega_{lk}^- t), \tag{27}$$

where

$$\omega_{lk}^\pm = (l \cos \theta \pm k \sin \theta) (2\pi v/a), \tag{28}$$

$$E_U(l, k) = \sum_h \left(\frac{\pi h}{a} \right) \Phi_{hkl} \times \begin{cases} (-1)^{\frac{1}{2}h} \sin(2\pi h b_U/a), & l \text{ even} \\ (-1)^{\frac{1}{2}(h-1)} \cos(2\pi h b_U/a), & l \text{ odd} \end{cases}, \tag{29}$$

$$E_W(l, k) = \frac{\pi l}{a} \sum_h \Phi_{hkl} \times \begin{cases} (-1)^{\frac{1}{2}h} \cos(2\pi h b_U/a), & l \text{ even} \\ (-1)^{\frac{1}{2}(h+1)} \sin(2\pi h b_U/a), & l \text{ odd} \end{cases}, \tag{30}$$

and

$$E_V(l, k) = (k/l) E_W(l, k). \tag{31}$$

The sums extend over all non-negative integers for which h , k , and l are all even or all odd.

Although the above analysis is applicable to any angle θ , we will discuss only cases in which θ is small enough that $\cos \theta \approx 1$. First, when $\theta = 0$, the expression for the frequencies reduces to $(2\pi v/a)l$, $l = 1, 2, 3, \dots$, which is (as it must be) just the same as for (001) axial channeling [Eq. (15)]. For small tilts, θ , we see from Eq. (28) that the even harmonics of (approximately) $(2\pi v/a)$ still occur, now flanked by sidebands displaced by even multiples of $\pm(2\pi v/a) \sin \theta$. On the other hand, the odd harmonics of $(2\pi v/a)$ become split into systems of only sidebands, located at frequencies $\pm k(2\pi v/a) \times \sin \theta$, $k = 1, 3, 5, \dots$ relative to the missing central peaks.

For trajectories in the midplane, the field direction is longitudinal at resonance for even harmonics (l even), while the field is perpendicular to the midplane for odd harmonics (l odd). These polarizations are essentially the same as for (001) axial channels.

IV. APPARATUS

The experimental arrangement is shown in Fig. 5. Ion beams of B , C , N , O , and F were obtained

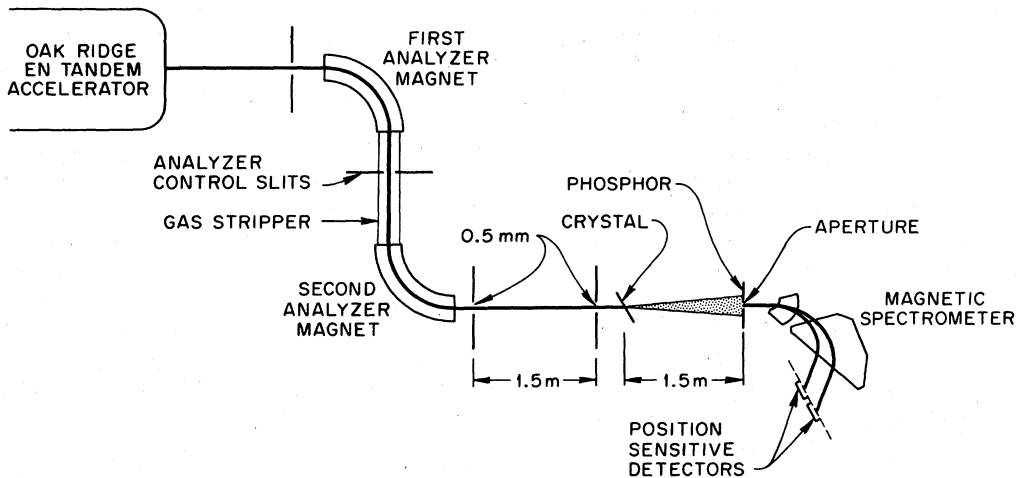


FIG. 5. Experimental arrangement.

from the Oak Ridge EN Tandem Accelerator. Usually the ions emerging from the first magnetic analyzer were not one-electron ions so they were passed through a gas stripper to the second magnetic analyzer which was used to select ions of the charge state required. Following the second magnetic analyzer, two apertures of 0.5 mm diameter, spaced 1.5 m apart were used to collimate the beam entering the crystal (a 1000-Å-thick Ag crystal and an 850-Å-thick Au crystal were used). Channeled particles emerging from the crystal were collimated by a 1 mm aperture 1.5 m downstream. A phosphor surrounding the final aperture was used to observe the emergent channeling pattern and to serve as a guide for crystal alignment. These patterns were observed to be ~ 1 cm in diameter in typical cases. It should be noted that the final collimator preselected particles which had very little transverse momentum in the crystal channels. These particles then passed into a split-pole magnetic spectrograph for charge-state separation and energy analysis. The spectrograph was fitted with two Si position-sensitive detectors whose spacing could be adjusted for detection of one-electron ions and bare nuclei. With such narrow collimation, the magnetic spectrograph had a collection efficiency of unity. Bare nuclei and one-electron ions were collected simultaneously so that beam current fluctuations did not affect the counting rate ratios.

Examination of the energy-loss spectra of the emerging one-electron ions usually reveals a group of ions which appear to have retained their charge state throughout their passage through the crystal. These ions cluster in a narrow band of energy loss, characteristic of the stopping power expected for an ion of $q = Z - 1$. In addition to these ions, others appear to have changed their charge several times but emerged with their original charge. Having spent varying fractions of their trajectories as bare ions, they appear in the spectra as a somewhat broader group of lower energy (higher energy loss). To illustrate these effects, we show in Fig. 6 three pairs of spectra obtained with a crystal slightly misoriented to produce a greater than usual population of particles which have changed their charge several times in passage. The three ratio numbers clearly show that the total one-electron-ion fraction passes through a minimum in a narrow range of particle velocity. Inspection of the energy-loss spectra of the one electron ions shows that the higher-energy (fixed-charge) peak is strongly depressed at the resonance. Analysis of the spectra in a few cases has always shown that particles outside the sharp peak do not show any resonant behavior.

The ratio calculated as shown will always under-

estimate the strength of the resonance effect. If the crystal had been correctly aligned to a $\langle 111 \rangle$ axis the number of particles outside the fixed-charge peak would have been much smaller and the shape changes would have been seen less clearly. In some examples, the subtraction of those particles which do not retain a fixed charge would not significantly alter the results obtained. In many cases, particularly for light ions, electron loss unassociated with coherent excitation is a prominent competing process. In a few cases both capture and loss may affect the shape of the resonance curves.

V. RESULTS

In Fig. 7 we display the total population fraction of N^{6+} ions emerging into our acceptance solid angle from an 850-Å-thick Au crystal as a function of incident energy. The spacing along a $\langle 111 \rangle$ row is 7.064 Å. Resonances are shown for $K=4, 5,$ and 6. Additional scales are given in terms of v/v_r , where v is incident velocity and v_r is the resonance velocity calculated for an isolated one electron ion. As we have shown in Fig. 6, the minima are deeper than those shown here because we include all particles rather than exclusively those which have minimum energy loss (indicative of fixed charge state). Calculated resonance positions for transitions to $n=2, 3,$ and 4 are shown by arrows on the abscissa. Similar data have been found for C^{5+} ions in $\langle 111 \rangle$ channels of gold.

We have observed a number of resonances; generally it can be said that: (i) the resonances are stronger for smaller harmonic numbers; (ii) the resonances usually fall at velocities slightly below the calculated values; (iii) the resonances are asymmetric; (iv) there appears to be a baseline trend downward with energy and it will be shown that this trend could indicate effects which would weaken the apparent strengths of the minima; (v) resonances indicative of transitions to states with $n \geq 3$ are relatively weak. More specifically, we have seen indications of ($n=1$) to ($n=3$) resonances but ($n=1$) to ($n \geq 4$) resonances lie entirely inside the statistical uncertainties of our data.

In order to discuss the baseline trends we compare the N^{6+} data of Fig. 7 with similar data recorded for C^{5+} in Fig. 8. Here R is the total fractional population of one electron ions and R^* is the fractional population of "group A" (i.e., the fraction remaining in a fixed charge state) as indicated in the inset. The resonant excitation manifests itself as an increase in the effective ionization cross section and hence a decrease in R or R^* at energies fulfilling the resonance condition [Eq. (2)]. Since R and R^* have been measured over a

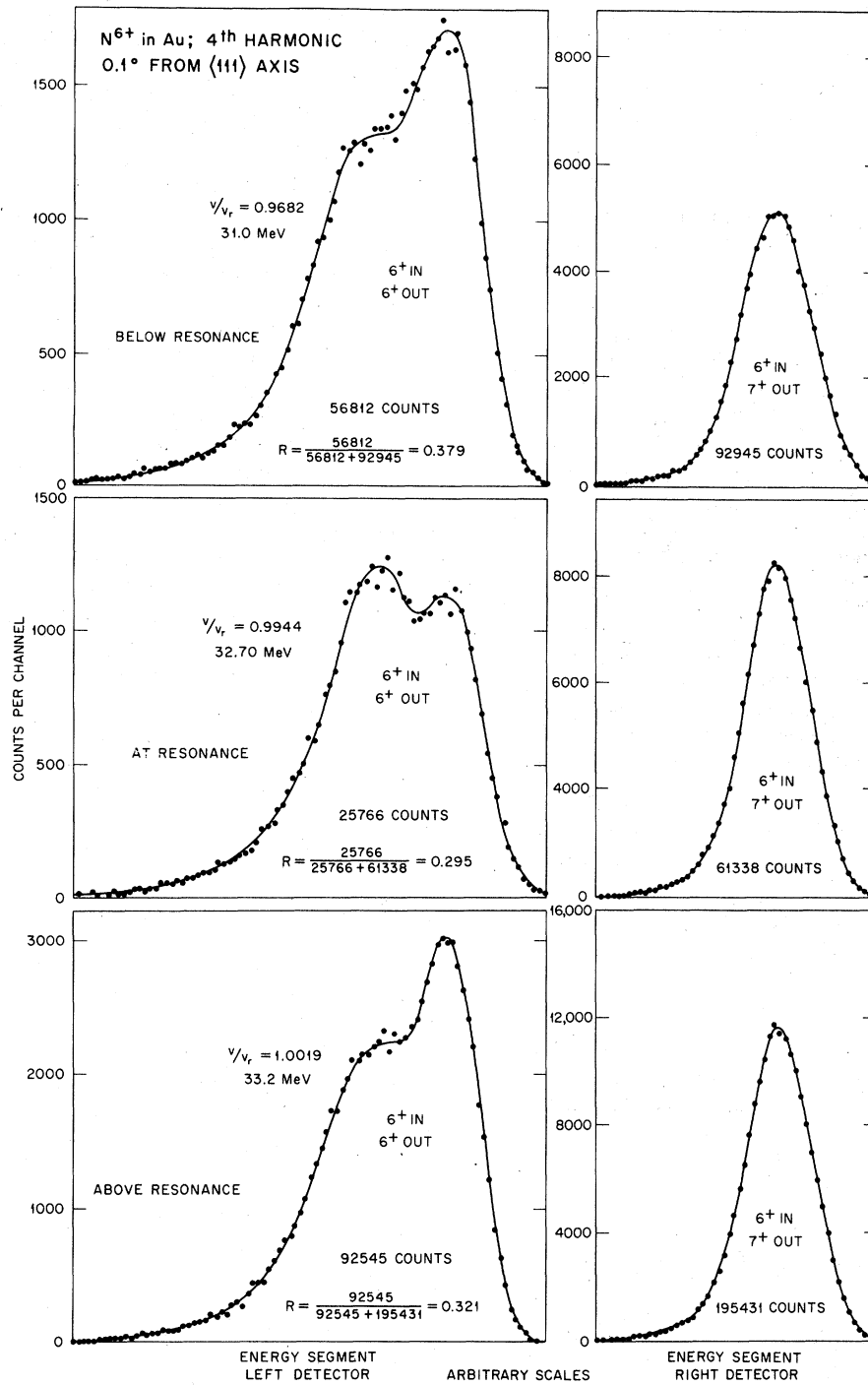


FIG. 6. Energy-loss spectra of N^{6+} and N^{7+} ions below, at, and above a coherent excitation resonance. Each pair of energy segments was recorded simultaneously on two Si position sensitive detectors.

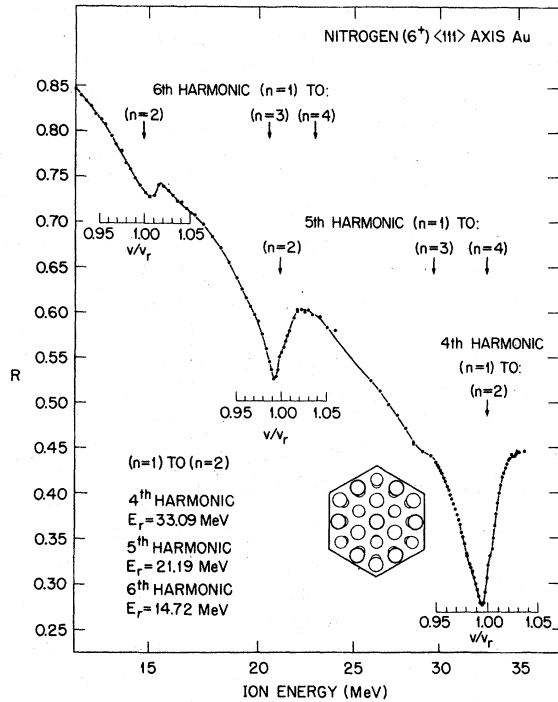


FIG. 7. Ratio R of N^{6+} counts to the sum of N^{6+} and N^{7+} counts as a function of initial energy for $\langle 111 \rangle$ axial channeling. The abscissa is linear in velocity. The incident beam is N^{6+} .

broad energy range in a $\langle 111 \rangle$ axis, one can obtain information from Fig. 8 about the energy dependence and magnitude of R and R^* in the absence of resonant excitation. In the following, the secular trend of R and R^* will be denoted R_S and R_S^* .

For both C and N , R_S decreases with increasing energy whereas R_S^* shows a relatively weak energy dependence for C but a strong decrease with energy for N . Furthermore, it should be noted that on an absolute scale R_S and R_S^* are larger for N than for C .

Since the capture cross sections for channeled ions are drastically reduced compared to those in amorphous targets³³ one can estimate R_S or R_S^* by considering electron loss and excitation to be the only important processes. In this case we assume that we are dealing with a three-component system consisting of ground-state one-electron ions (i), one-electron ions in the $n=2$ state (i^*), and bare nuclei (f). The fraction of one-electron ions after passage through the crystal can now be found by solving the following set of differential equations:

$$\frac{dF_i(\pi)}{d\pi} = -F_i(\pi)(\sigma_{if} + \sigma_{ii^*}) + F_{i^*}(\pi)\sigma_{i^*i}, \quad (32)$$

$$\frac{dF_{i^*}(\pi)}{d\pi} = F_i(\pi)\sigma_{ii^*} - F_{i^*}(\pi)(\sigma_{i^*f} + \sigma_{i^*i}), \quad (33)$$

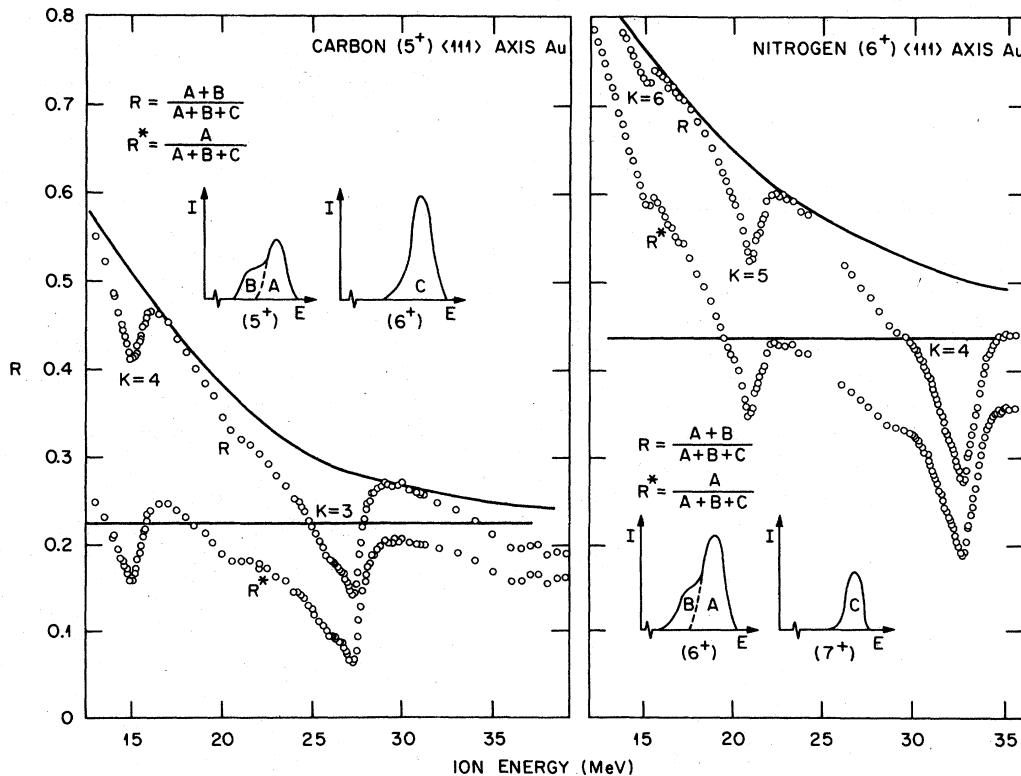


FIG. 8. Effect of energy variations of capture, loss, and excitation cross sections upon the nonresonant one-electron ion population. The lower solid curves include only ionization effects. The upper solid curves include electron capture.

$$F_i(\pi) + F_{i*}(\pi) + F_f(\pi) = 1, \quad (34)$$

$$F_i(0) = 1. \quad (35)$$

Here π is the target thickness, F_a is the fraction of projectiles in state a and σ_{ab} is the cross section for going from state a to state b in a single collision. Electron loss and excitation are assumed to take place in collisions between the moving ions and essentially free conduction electrons. We have used ionization and excitation cross sections derived from Golden and Sampson's^{34,35} semiempirical formula.

Let us consider as an example 35-MeV carbon. Here the cross sections per electron are $\sigma_{56} = 9.3 \times 10^{-20} \text{ cm}^2$, $\sigma_{55*} = 7.9 \times 10^{-20} \text{ cm}^2$, $\sigma_{5*6} = 2 \times 10^{-18} \text{ cm}^2$, and $\sigma_{5*5} = 2 \times 10^{-20} \text{ cm}^2$. Note here that excitation to the $n=2$ state effectively supplies an additional ionization channel. This has two effects. First, it makes F_i almost independent of energy since σ_{ii*} and σ_{if} as well as σ_{i*f} are almost constant over the energy region investigated and second, it produces a decrease of F_i when an additional excitation channel is turned on at resonance energies. We should note here that the number of free electrons per target atom is used as a fitting parameter. If the number of electrons per atom is taken as 18, we find that $F_5 = 0.22$ and $F_{5*} = 0.01$ in good agreement with experimental results. The somewhat unrealistically high value of electron density may reflect an underestimate of the cross sections of $\lesssim 50\%$ or it may be due to the rather crude approximation. With this approximation one obtains values of F_i plus F_{i*} shown as the horizontal lines on Fig. 8; it apparently gives a reasonable agreement with R_S^* for carbon and at high energies for nitrogen. The larger absolute value for nitrogen reflects a decrease in the electron-loss cross section ($\sigma \propto Z_1^{-4}$) as we go from carbon to nitrogen.

In order to obtain a better agreement with experiments for nitrogen, electron capture must be included. The upper curves of Fig. 8 are obtained by incorporating capture by bare nuclei to the ground state of the one-electron ion. The capture cross sections are fitted to give overall good agreement with R_S . The capture cross sections per electron thus determined agree within 20% with those measured by Macdonald and Martin³⁶ for He when divided by two to account for the two electrons.

The difference in behavior of R_S^* for C compared to N results from the fact that a carbon ion which loses and then captures an electron has an energy loss which no longer corresponds to that of group A while nitrogen ions, which capture more quickly because of the larger cross section, still will fall in the A group. When capture is an important fac-

tor, the shapes, positions and strengths of resonances may all be affected. In the extreme case of very large capture cross sections, particles which have been coherently excited and ionized will immediately capture an electron and rejoin the low-energy loss group of one-electron ions. Such an effect would reduce the depth of the minimum.

Two causes for the correlation of large harmonic numbers with weak resonances are thermal motion effects⁴ and the fact that, as we have shown here, the matrix elements for the excitations tend to become smaller for higher harmonic numbers.

The resonance velocity is usually slightly less than that calculated; the ΔE_{12} energy spacing is reduced because of the static fields in the crystal. An asymmetric resonance could be caused by differences in the electric field encountered by particles with slightly different paths along the channel, giving rise to a spectrum of ΔE_{ij} values which has an upper limit for ions which pass exactly along the center line of a channel.

The relative weakness of $(n=1) \rightarrow (n \geq 3)$ resonances may be due to very large level widths for the upper state caused by its greater sensitivity to variations in the electric field and to the very short collisional lifetimes for these states.

In Fig. 9 we present a schematic representation of the effect of tilting the strings of atoms a small amount (in this case 0.7°) with respect to the direction of the ions. If the crystal is tilted from a $\langle 100 \rangle$ axis along a $\{100\}$ planar direction, the ions can continue to avoid the strings, but as they pass from midway between two strings to midway between the next two strings, etc., then excitation is modulated at a rate which corresponds to a beat frequency of $\nu_0 k l^{-1} \tan \theta$, where ν_0 is the original unmodulated frequency, θ is the tilt angle, l is the harmonic number, and k is an integer which is odd if l is odd, and even if l is even. For small angles θ , this is in agreement with Eq. (28) and has been discussed in Sec. III E. In the example of Fig. 9, the resonance is shown with upper and lower sidebands of $\nu_0 \pm 0.004\nu_0$. The presence or absence of a central minimum accompanying the sidebands depends on whether the harmonic is even or odd. For the odd-harmonic case, where the excitation is primarily transverse, the absence of the central minimum occurs because the phase of the excitation reverses each time an ion steps from one channel into an adjacent channel.

In Fig. 10 we present curves which illustrate the sideband effect. In this case we show a third (odd) harmonic excitation of O^{7+} ions. The splitting is seen to be proportional to the angle of tilt and the shifts in velocity agree quantitatively with the relation $\Delta v/v_0 = \Delta \nu/\nu_0 = \frac{1}{3} \tan \theta$. The small angles in-

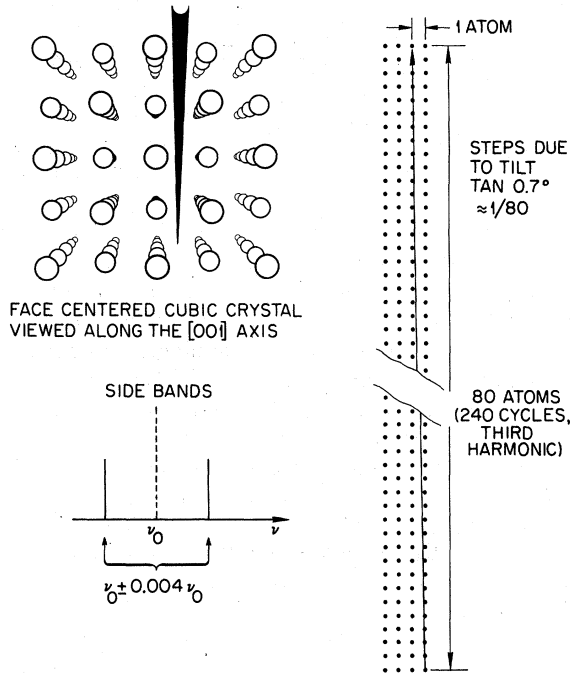


FIG. 9. Effect of a small tilt upon a third harmonic resonance.

involved foreshorten the string spacing by a factor $(1 - \cos\theta)$, which is twenty times less than the observed resonance shifts. For the larger tilts of Fig. 10 the beam direction is completely out of the axial channel and resonant coherent excitation in planar channels occurs. The case illustrated corresponds to Eq. (28) for $l=3$ and $k=1$. The $k=3$ sidebands are weaker and were not identified in the present data.

The moving ion induces a polarization of the medium and the field resulting from this polarization has a constant nonzero component in the longitudinal direction. This field which is related to the stopping-power Stark splits the $n=2$ manifold into three states. The central substate, which is unshifted in first order, is composed of a $2p_x, 2p_y$ degenerate mixture, while the outer two states arise from mixtures of the $2s, 2p_x$ states. Transverse oscillating fields will excite the degenerate $2p_x, 2p_y$ state; longitudinal oscillating fields will excite the outer $2p_x, 2s$ pair of substates. For even harmonics in the case of $\langle 001 \rangle$, for all harmonics in the case of $\langle 110 \rangle$ channels, and for harmonics which are multiples of three in the case of $\langle 111 \rangle$ channels, the oscillating fields are predominantly longitudinal. In these cases one expects to observe double minima. An example of such a double minimum is shown in Fig. 11.

The behavior of an even harmonic resonance

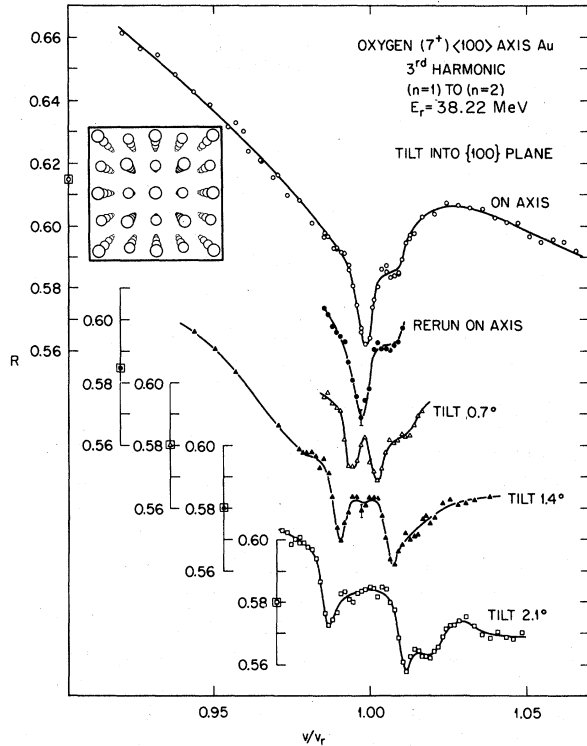


FIG. 10. R vs v/v_r , where R is ratio of O^{7+} counts to the sum of O^{7+} and O^{8+} counts, and v/v_r is velocity in units of the calculated resonance velocity. Incident beam O^{7+} . Four crystal orientations. Tilt along $\{100\}$ planar channel from $\langle 001 \rangle$ axis in Au.

with tilt is in marked contrast to that shown in Fig. 10. In Eq. (28), k and l are both even (or both odd). For the case $l=2$, the lowest-order term is $k=0$. For small angles the frequency ω_{20} is affected only by string foreshortening. In Fig. 12 we demonstrate that tilting the crystal produces very little effect upon the positions of the minima; in this case, the minima were observed for N^{6+} ions. The resonance observed at 0° is somewhat different from those observed at 0.7° , 1.4° , and 2.1° . Examination of the energy-loss spectra has shown that, for the 0° case, some of the particles have been hyperchanneled.³⁰ The difference in energy loss for this group of particles is too small for a clear separation to be seen in our spectra because energy straggling has a serious mixing effect for very thin crystals. A partial separation indicates that hyperchanneled particles are not excited as readily as the rest. This is to be expected since hyperchanneled particles remain close to the channel axis where the matrix elements of the interactions with the crystal field are smallest (see Fig. 2). The separation of the minima of Fig. 12 is a measure of the wake field in the vicinity of the

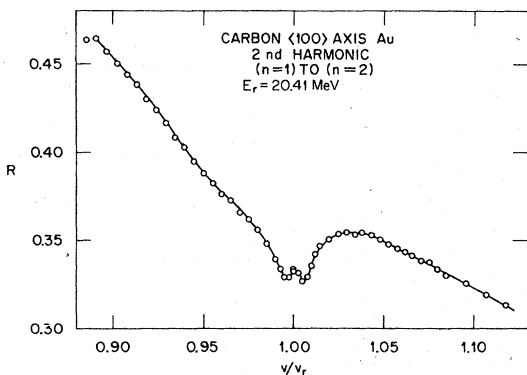


FIG. 11. R vs v/v_r , where R is ratio of C^{5+} counts to the sum of C^{5+} and C^{6+} counts, and v/v_r is velocity in units of the calculated resonance velocity. Incident beam was C^{5+} . Second harmonic. $\langle 100 \rangle$ axis in Au.

moving ion. The separations to be expected will be discussed in a later publication.²⁴

In Fig. 12 we have seen that tilts of up to 2.1° along a $\{100\}$ planar channel do not seriously attenuate the resonance. In contrast to this, Fig. 13 shows the result of a 1° tilt along a $\{110\}$ planar channel; here the resonance has been very seri-

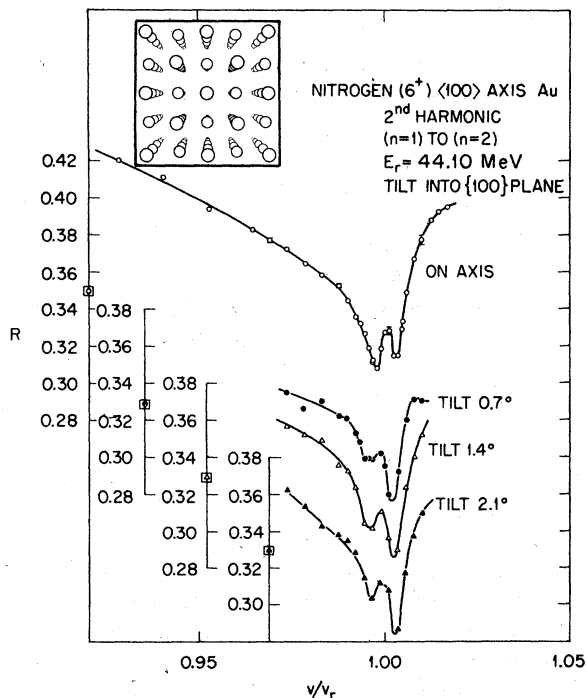


FIG. 12. R vs v/v_r , where R is ratio of N^{6+} counts to the sum of N^{6+} and N^{7+} counts, and v/v_r is velocity in units of the calculated resonance velocity. Four orientations of the crystal. Incident beam was N^{6+} . Tilt along a $\{100\}$ planar channel from $\langle 100 \rangle$ axis in Au.

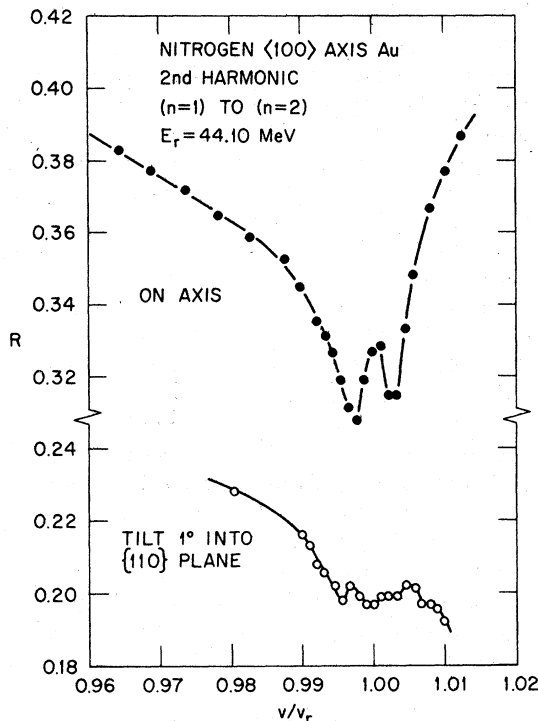


FIG. 13. Attenuation of resonance due to small tilt from $\langle 100 \rangle$ axis along a $\{110\}$ planar channel. R vs v/v_r , where R is ratio of N^{6+} counts to the sum of N^{6+} and N^{7+} counts, and v/v_r is velocity in units of the calculated resonance velocity. Incident beam was N^{6+} .

ously attenuated. Examination of the energy-loss spectra showed that, in this planar channel, very few particles remained in the low-energy-loss group. The narrower spacing of $\{110\}$ planar channels introduces so much electron loss and capture that the one-electron-nitrogen ions do not hold fixed charge long enough for coherent excitation to take place.

We have made attempts to observe resonant coherent excitation in the $\langle 110 \rangle$ axial channels of Au and Ag, and we find that generally the resonances are quite weak and the calculated matrix elements for these are smaller because $\langle 110 \rangle$ channels are very large. An example is the 42.99 MeV even harmonic resonance for O^{7+} in a $\langle 110 \rangle$ axis of Au shown in Fig. 14. The minimum is less than 5% in depth and the details of this second-harmonic resonance are not clear. The drawing of the channels of the face-centered cubic crystal in Fig. 15 serves to give a quantitative comparison of distances in the channels. For particles along center lines of planar and axial channels in Au, the distances to the nearest atoms are: (i) $\langle 110 \rangle$ axes 1.442 Å (and 2.039 Å, alternating); (ii) $\langle 100 \rangle$ axes

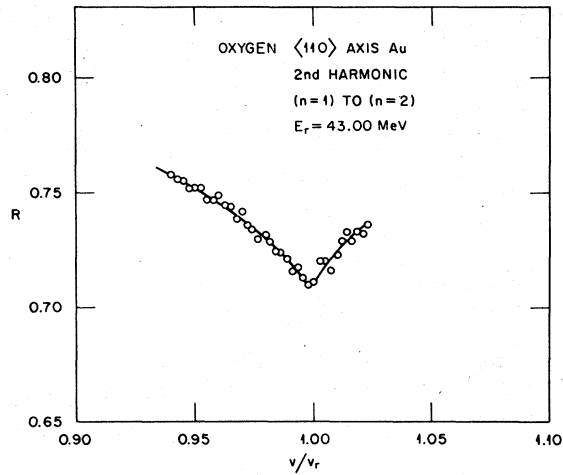


FIG. 14. R vs v/v_r , where R is ratio of O^{7+} counts to the sum of O^{7+} and O^{8+} counts, and v/v_r is velocity in units of the calculated resonance velocity. Incident beam was O^{7+} . Second harmonic. $\langle 110 \rangle$ axis in Au. Depth of minimum $\sim 5\%$.

1.442 Å (and 1.442 Å, alternating); (iii) $\{100\}$ planes 1.019 Å; (iv) $\langle 111 \rangle$ axes 0.961 Å (at 0° , 120° , 240° in perpendicular plane, repeating); (v) $\{110\}$ planes 0.721 Å.

The tentative conclusion is that, if the particles remain too far from nearest atoms, coherent excitation is weak; if they remain too close to nearest atoms, capture and loss occur so frequently that coherent excitation cannot occur. Thus, for ions of nitrogen in our energy range, excitation is weak for distances ≥ 1.4 Å and ion-charge change is too frequent for distances ≤ 0.75 Å. In the range between 0.75 Å and 1.4 Å, coherent excitation gives strong resonance effects.

Our experience indicates that the $\langle 111 \rangle$ axes produce strongest resonances, and $\langle 110 \rangle$ axes produce weakest resonances. It has been pointed out that in $\langle 111 \rangle$ channels, for trajectories exactly on the channel axes the harmonics, which are divisible by three, are longitudinal. Close inspection of the carbon data shown in Fig. 8 shows that the third harmonic resonance at 27.2 MeV has a shape which is indicative of a double minimum where the left minimum is at ~ 25.8 MeV or 2.6% lower in velocity, a splitting which is approximately four times that observed for the second-harmonic resonance with nitrogen ions in $\langle 100 \rangle$ axial channels. It is not known why the minima are poorly resolved, and this prevents an accurate determination of the separation.

In Figs. 16 and 17 we present data for both one- and two-electron ions of fluorine in $\langle 100 \rangle$ channels, respectively. Again the even (fourth) harmonic

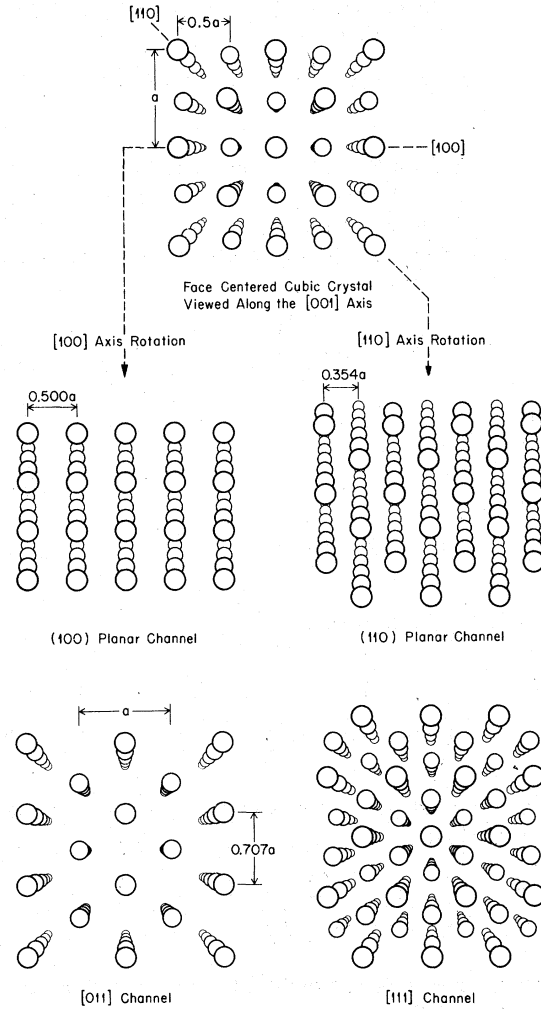


FIG. 15. Channels for face centered cubic crystal.

excitation of the one-electron ion appears to be a double minimum and the resonances are rather weak as expected from the fields shown in Fig. 3. Since the ionization cross section of the $n=2$ electrons becomes smaller with increasing Z_1 ($\sigma \propto Z_1^{-4}$), fewer of the ions which have been coherently excited will be ionized. If this is the case, fluorine ions might be observed to emit x-rays after passage through the crystal.

If x-rays can be observed from heavier ions, their polarization may give additional information about crystal fields and wake fields. Two additional classes of resonant transitions may be studied. The first is the inverse of the set of reactions reported here; bare ions first capture an electron into an excited state of the one-electron ion and this is followed by downward coherent de-excitation. The second example is the case where an electron is captured into an ionic ground state

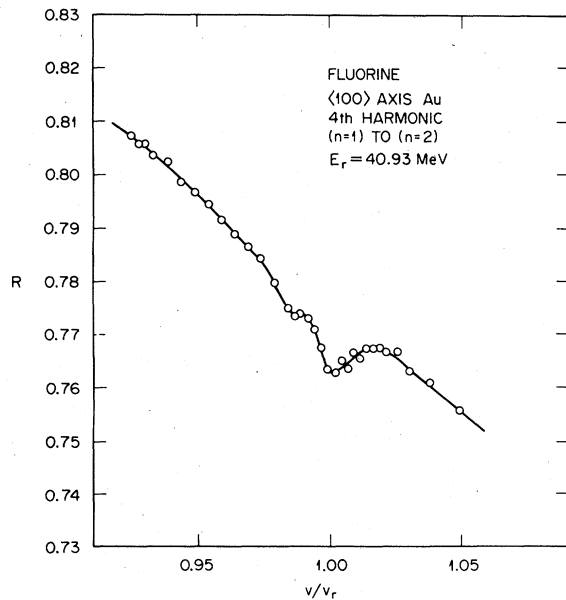


FIG. 16. R vs v/v_r , where R is ratio of F^{8+} counts to the sum of F^{8+} and F^{9+} counts, and v/v_r is velocity in units of the calculated resonance velocity. Incident beam was F^{8+} . Fourth harmonic. $\langle 100 \rangle$ axis in Au.

and then coherently excited and ionized. In general, resonant coherent interactions may provide alternative paths for various radiative or nonradiative interactions. With very heavy ions of sufficiently small shell radii, multiple electron ions may be used in resonant coherent interaction experiments. In planar channeling studies the sideband effect will increase the number of minima to be observed in a given range of bombarding energies. The widths and asymmetries of the resonances require further study. Other details can be seen in the resonances reported here but the data are not sufficiently accurate to permit analysis. Our calculations indicate that resonances in Ag crystals are expected to be slightly weaker than the same resonances in Au crystals and our data agree with this prediction.

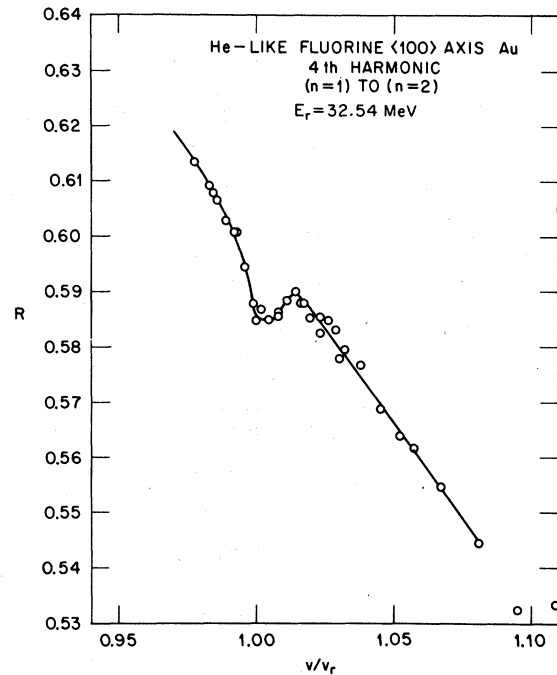


FIG. 17. R vs v/v_r , where R is ratio of F^{7+} counts to the sum of F^{7+} and F^{8+} counts, and v/v_r is velocity in units of the calculated resonance velocity for the transition $1s^2 \rightarrow 1s2p$. Incident beam was F^{7+} . Fourth harmonic. $\langle 100 \rangle$ axis in Au.

ACKNOWLEDGMENTS

We would like to thank R. H. Ritchie, I. L. Thomas, and J. S. Briggs for helpful discussions, and D. Gemmell of Argonne National Laboratory and J. Chevalier of Aarhus University for supplying the Au and Ag crystals used in the experiments. Research for this work sponsored by the Division of Physical Research, U. S. Department of Energy, under Contract No. W-7405-eng-26 with Union Carbide Corporation.

*Permanent address: Institute of Physics, University of Aarhus, Aarhus, Denmark.

¹S. M. Smith and E. M. Purcell, *Phys. Rev.* **92**, 1069 (1953).

²F. J. Dyson and H. Überall, *Phys. Rev.* **99**, 604 (1955).

³H. Überall, *Phys. Rev.* **103**, 1055 (1956).

⁴V. V. Okorokov, *Pis'ma Zh. Eksp. Teor. Fiz.* **2**, 175 (1965) [*JETP Lett.* **2**, 111 (1965)].

⁵V. V. Okorokov, *Yad. Fiz.* **2**, 1009 (1965) [*Sov. J. Nucl. Phys.* **2**, 719 (1966)].

⁶T. Hadeishi, W. S. Bickel, J. D. Garcia, and H. G.

Berry, *Phys. Rev. Lett.* **23**, 65 (1969).

⁷T. Hadeishi, *Nucl. Instrum. Methods* **90**, 337 (1970).

⁸V. V. Okorokov, D. L. Tolchenkov, I. S. Khizhnyakov, Yu. N. Cheblukov, Yu. Ya. Lapitsky, G. A. Iferov, and Yu. I. Zhukova, *Pis'ma Zh. Eksp. Teor. Fiz.* **16**, 588 (1972) [*JETP Lett.* **16**, 415 (1972)]; *Phys. Lett.* **43**, 485 (1973).

⁹M. J. Gaillard, J. C. Poizat, J. Remillieux, and M. L. Gaillard, *Phys. Lett. A* **45**, 306 (1973).

¹⁰J.-C. Poizat and M. J. Gaillard (private communication to authors of Ref. 14).

- ¹¹Jun Kondo, J. Phys. Soc. Jpn. **36**, 1406 (1974).
- ¹²N. P. Kalashnikov and S. G. Pankratov, Sov. Phys. Solid State **16**, 542 (1974).
- ¹³S. Shindo and Y. H. Ohtsuki, Phys. Rev. B **14**, 3929 (1976).
- ¹⁴H. G. Berry, D. S. Gemmell, R. E. Holland, J.-C. Poizat, J. Remillieux, and J. N. Worthington, Phys. Lett. A **49**, 123 (1974).
- ¹⁵D. S. Gemmell (private communication).
- ¹⁶M. Mannami, H. Kudo, M. Matsushita, and K. Ishii, Phys. Lett. A **64**, 136 (1977).
- ¹⁷J. Golovchenko, W. M. Gibson, N. H. Tolk, and T. S. Noggle (private communication).
- ¹⁸D. Burch and A. D. Marwick, AERE Report M2742, Atomic Energy Research Establishment, Harwell, England, Sept. 1975 (unpublished).
- ¹⁹S. Datz, C. D. Moak, O. H. Crawford, H. F. Krause, P. F. Dittner, J. Gomez del Campo, J. A. Biggerstaff, P. D. Miller, P. Hvelplund, and H. Knudsen, Phys. Rev. Lett. **40**, 843 (1978).
- ²⁰C. D. Moak, S. Datz, B. R. Appleton, J. A. Biggerstaff, M. D. Brown, H. F. Krause, and T. S. Noggle, Phys. Rev. B **10**, 2681 (1974).
- ²¹S. Datz, J. Gomez del Campo, P. F. Dittner, P. D. Miller, and J. A. Biggerstaff, Phys. Rev. Lett. **38**, 1145 (1977).
- ²²J. D. H. Donnay and H. M. Ondik, *Crystal Data Determinative Tables*, 3rd ed. (U.S. Department of Commerce, Washington, 1973), Vol. II, p. C-44.
- ²³N. Bohr, Mat. Fys. Medd. Dan. Vid. Selsk. **18**, 71 (1948).
- ²⁴O. H. Crawford and R. H. Ritchie (unpublished).
- ²⁵O. H. Crawford (unpublished).
- ²⁶Cf. D. R. Bates, *Quantum Theory I. Elements* (Academic Press, New York, 1961), pp. 252-270.
- ²⁷We are concerned with transitions between the (totally symmetric) ground state, and excited states constructed from a basis of only *s* and *p* functions. In this case, dipole selection rules are exact, and symmetry-related conclusions are not in the least affected by ignoring the variation of the crystal field over the spatial domain of the ion-wave functions.
- ²⁸H. Hellmann, *Einführung in die Quantenchemie* (Deuticke, Leipzig, 1937), pp. 285-286; R. P. Feynman, Phys. Rev. **56**, 340 (1939).
- ²⁹*International Tables for X-Ray Crystallography*, edited by N. F. M. Henry and K. Lonsdale (Kynoch Press, Birmingham, 1952), Vol. I, p. 517.
- ³⁰B. R. Appleton, C. D. Moak, T. S. Noggle, and J. H. Barrett, Phys. Rev. Lett. **28**, 1307 (1972).
- ³¹G. Molière, Z. Naturforsch. **2A**, 133 (1947). For comparisons of this potential with some deduced from channeling experiments, see M. T. Robinson, Phys. Rev. B **4**, 1461 (1971); W. M. Gibson and J. Golovchenko, Phys. Rev. Lett. **28**, 1301 (1972).
- ³²A. Erdélyi, W. Magnus, F. Oberhettinger, and F. G. Tricomi, *Tables of Integral Transforms* (McGraw-Hill, New York, 1954), Vol. I, p. 17.
- ³³S. Datz, F. W. Martin, C. D. Moak, B. R. Appleton, and L. B. Bridwell, Rad. Eff. **12**, 163 (1972).
- ³⁴L. B. Golden and D. H. Sampson, Astrophys. J. **170**, 181 (1971).
- ³⁵L. B. Golden and D. H. Sampson, J. Phys. B **10**, 2229 (1977).
- ³⁶J. R. Macdonald and F. W. Martin, Phys. Rev. A **4**, 1965 (1971).